ChemComm

COMMUNICATION

View Article Online
View Journal | View Issue

Cite this: *Chem. Commun.*, 2023, **59**, 6024

Received 15th February 2023,
Accepted 20th April 2023

DOI: 10.1039/d3cc00719g

rsc.li/chemcomm

Chirality in luminescent $Cs_3Cu_2Br_5$ microcrystals produced *via* ligand-assisted reprecipitation†

Lorenzo Branzi, *[ab] Aoife Kavanagh, [b] Michele Back, [a] Adolfo Speghini, *[c] Yurii K. Gun'ko *[b] and Alvise Benedetti *[a]

Herein we report new chiral luminescent $Cs_3Cu_2Br_5$ needle-like microcrystals and the analysis of their optical properties and the effect of the ligand structure on the transfer of chirality.

The introduction of chiroptical activity in inorganic nanomaterials has recently attracted increasing interest due to the wide range of applications as well as the large scientific interest in the design of novel inorganic synthesis, which allows controlling the symmetry breaking.[1–4] During the last decade, extensive research activity on chiral lead halide perovskites $APbX_3$ (where A is a monovalent cation and X is a halide anion) has led to the observation of chirality in both all-inorganic (A = Cs^+)[5–7] and hybrid organic–inorganic (A = chiral organic cation, often α-methylbenzyl ammonium (MBA))[8–10] perovskites showing outstanding chiroptical properties with strong circular dichroism (CD) and circularly polarised luminescence (CPL) activities. Due to the toxicity and stability issues related to lead halide perovskite, several other lead-free perovskite and perovskite inspired materials have been extensively investigated in the last decade.[11,12] Among them, cesium copper halides are an emerging class of perovskite-inspired materials with promising applications in photonics.[13] Due to their optical properties and stability in environmental conditions, these materials have recently become the focus of extensive investigation as much less toxic alternatives to the most commonly studied lead halide perovskite, for several technological applications.[13–15] Possible applications of cesium copper halides as active materials for light emitting diodes (LEDs),[16–18] UV photodetectors,[19–21] scintillators[22–25] and lasing[26] have been investigated in recent years.

Recently, Cu(II)-based chiral hybrid organic–inorganic layered copper halides $(R/S\text{-MBA})_2CuCl_4$ and $(R/S\text{-MBA})_2CuBr_4$ have been reported in the literature as spin filters and second harmonic generators.[27,28] Recently, Ge *et al.*[29] reported a Cu(I)-based hybrid organic–inorganic halide $(R/S\text{-MBA})CuBr_2$ with superior non-linear optics performance. Despite the promising optical properties observed in hybrid copper-based halides, to the best of our knowledge, chirality has never been observed in all-inorganic copper halides.

In this report we demonstrate the successful chiral induction in all-inorganic $Cs_3Cu_2Br_5$ *via* a facile one step ligand-assisted reprecipitation (LARP) synthesis. This method allows for the production and isolation of highly crystalline needle-like microcrystals that present a strong CD activity and a photoluminescence quantum yield (PLQY) of 12.5%.

In this study, a synthesis based on the ligand-assisted reprecipitation (LAPR) process is developed to produce $Cs_3Cu_2Br_5$ needle-like microcrystals using L/D-arginine (Arg) as a chiral ligand. The procedure is based on the solubilisation of the metal precursors ($CuBr_2$ and CsBr) in DMF in the presence of L/D-Arg. Hydrobromic acid is employed to facilitate the solubilisation of the metal salts. The formation of Cu(I) ions is triggered *in situ* by the addition of thioglycolic acid that quickly reduces Cu(II) ions. Crystallisation of the metal halide phase is then induced at room temperature by the dropwise addition of the precursor solution in iso-propyl alcohol, which acts as an antisolvent. Performing the reaction at higher temperatures (*e.g.* under reflux conditions) gives the formation of larger crystals with poor colloidal stability and chiroptical activity.

The crystallographic phase has been confirmed by X-ray diffraction (XRD) analysis. XRD patterns of the samples prepared in the presence of L-Arg (L-CCB) and D-Arg (D-CCB) show good agreement with the reference pattern (Fig. 1), confirming the production of the desired orthorhombic *Pnma* phase. The absence of any diffraction peaks related to the CsBr reagent further confirms the purity of the product. Moreover, since no diffraction features related to the arginine crystals can be detected, the presence of a chiral ligand impurity related to the arginine coprecipitation can be excluded.

[a] *Department of Molecular Science and Nanosystems, Ca' Foscari University of Venice, Via Torino 155 Venezia Mestre, Venezia, VE, Italy*
[b] *School of Chemistry, CDT ACM, CRANN and AMBER Research Centres, Trinity College Dublin, College Green, Dublin 2, Ireland. E-mail: Branzil@tcd.ie*
[c] *Nanomaterials Research Group, Department of Biotechnology and INSTM, RU of Verona, University of Verona, Strada le Grazie 15, Verona, Italy*

† Electronic supplementary information (ESI) available. See DOI: https://doi.org/10.1039/d3cc00719g

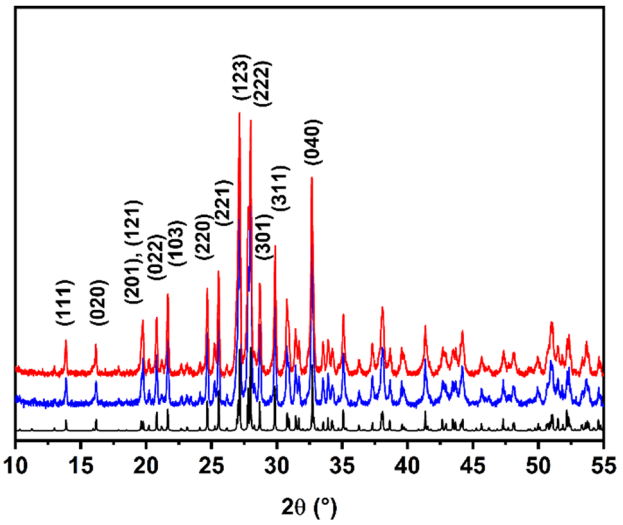

Fig. 1 XRD pattern of L-CCB (blue), D-CCB (red) and the reference pattern of orthorhombic $Cs_3Cu_2Br_5$ (black) according to the reported data ICSD22950.

SEM micrographs reported in Fig. 2a show the presence of micrometrical needle-like crystals with a broad size distribution. Moreover, several larger anisotropic crystals made by clusters of merged smaller crystals can be observed at higher magnification in Fig. 2b–d. The average length and width of the microneedles are about 5 μm and 100 nm, respectively (Fig. S1, ESI†). A similar anisotropic shape related to $Cs_3Cu_2Br_5$ crystals, prepared by a one-pot method, was also reported by Li *et al.*[30] For L-CCB microwires, the relative composition of 3.1 : 2.0 : 5.7 for Cs, Cu and Br, respectively, is estimated by energy dispersive X-ray spectroscopy (EDS). The observed values are close to the stoichiometric composition with an excess of bromide related to the synthetic conditions. Despite the high level of noise, due to the sample thickness, the elemental mapping (Fig. S2, ESI†) shows a homogeneous distribution across the crystal.

Further details on the structure of the L-CCB microcrystals are collected by TEM analysis (Fig. 3). The analysis confirms the structure of the larger crystals, which are composed of a cluster

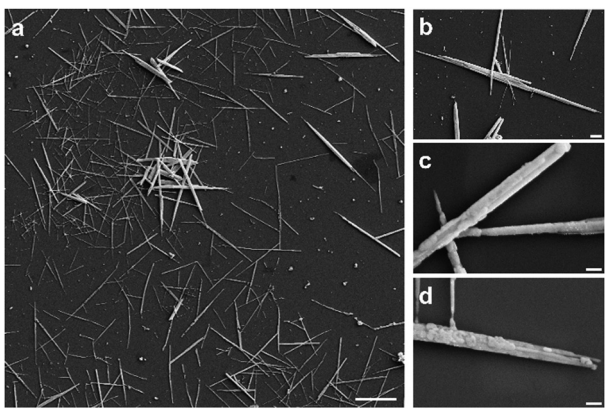

Fig. 2 (a–d) SEM images of L-CCB; scale bars: (a) 2.0 μm, *b* = 1.0 μm and *c* and *d* = 200 nm.

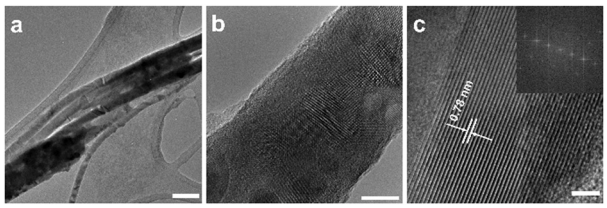

Fig. 3 TEM investigation of L-CCB, (a) morphological details of a crystal composed by multiple microwires, (b and c) phase contrast analysis of a single microwire. (c) Inset: FFT analysis of the diffraction pattern. Scale bars: *a* = 100 nm, *b* = 10 nm, and *c* = 5 nm.

of smaller needle-like crystals (Fig. 3a). The magnification of the structure of a single microwire is reported in Fig. 3b and c. Phase contrast analysis of a single needle-like crystal shows the high crystallinity of the system and the fast Fourier transform (FFT) analysis of the fringes (Fig. S3, ESI†) reveals a *d*-spacing of 0.78 nm related to the (101) diffraction of the orthorhombic phase of $Cs_3Cu_2Br_5$. This analysis suggests that the preferential growth direction of the crystals, during the antisolvent assisted recrystallisation, occurs along a crystallographic direction perpendicular to (101). As already observed for other metal halides, the specimen is very sensitive to the irradiation of the electron beam. In addition to a significant thermal decomposition of the crystals, after a short exposition under the electron beam, the formation of spherical nanoparticles on the surface and inside the nanocrystal itself can be observed (Fig. S4, ESI†). A similar behavior is commonly observed for lead halides.[31] However, despite their sensitivity under the electron beam, the material shows a remarkable stability when stored in air at room temperature. Indeed, the XRD analysis of powder samples stored in air for two months shows no sign of degradation (Fig. S5, ESI†).[14]

UV/Vis absorption analysis (Fig. 4a) of the L-CCB dispersion in iso-propyl alcohol shows the presence of a band with a maximum of around 300 nm (4.1 eV) that can be related to the band-edge absorption of $Cs_3Cu_2Br_5$.[32] The strong contribution of the tail, observed at longer wavelength, is likely related to a scattering process associated with the micrometrical size of the microwires. The photoluminescence (PL) of the prepared $Cs_2Cu_3Br_5$ is investigated in an iso-propyl alcohol dispersion (Fig. 4b). The PL profile shows an emission band centred at 460 nm (2.69 eV) with a full width half maximum of 87 nm (505 meV). The photoluminescence excitation (PLE) analysis reveals a narrow excitation band centred at around 283 nm

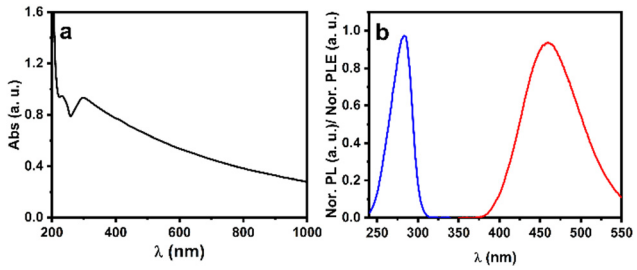

Fig. 4 (a) UV/Vis absorption spectrum and (b) PL (red) and PLE (blue) spectra of the L-CCB colloidal dispersion in iso-propanol.

(4.38 eV) and a large Stokes shift of 177 nm (1.69 eV). These findings are in good agreement with the values presented by other authors on $Cs_3Cu_2Br_5$ prepared *via* different approaches such as mechanochemical synthesis.[33,34] A PLQY of 12.5% is estimated by comparison with a tryptophan solution in deionised water. The obtained PLQY value is in line with other values reported on $Cs_3Cu_2Br_5$.[34,35] The large Stokes shift indicates a radiative relaxation *via* a self-trapped excitation (STE) mechanism. STE emission is the principal process observed in structures like 0D metal halides where, in addition to strong electron–phonon coupling, the exciton is localised in the metal halide clusters that, due to the lack of an interconnected coordination network, are easily distorted.[36]

The presence of chiral ligand molecules in $Cs_3Cu_2Br_5$, produced by the LARP method has been investigated by FTIR analysis (Fig. S6, ESI†) comparing the L/D-CCB infrared absorption spectrum with those of L-arginine and a bulk $Cs_3Cu_2Br_5$ sample prepared without the addition of ligands (named bulk-CCB). All the cesium copper bromide samples are characterised as dry powders after purification. Despite the low intensity of all the FTIR peaks observed for both L and D-CCB samples, the presence of a broad peak centred at around 3340 cm^{-1} can be related to νNH and νOH of the ammonium cations and the carboxylic groups. The peaks at 2970 and 2915 cm^{-1} can be attributed to νCH sp^3 in the methylene chain. The distinctive signals at 1730 and 1656 cm^{-1} are related to the νCOOH of the protonated carboxylate group and to the symmetric νCN_3 of the guanidinium hydrobromide followed by a broad band of the δNH.[37,38] The broad band between 1000 and 1130 cm^{-1} can be related to the νCN of the primary ammonium group. The observed signals prove that the ligand is still bound to the copper halide particle surface after the purification step in its cationic form.

The transfer of chirality is investigated by electronic circular dichroism (Fig. 5). The successful induction of chirality is confirmed by a CD-active transition in the band-edge region at around 310 nm. The observation of the opposite signal, according to the chirality of the chiral ligand, highlights the enantioselectivity of the synthesis. The transition in the band-gap region has a positive CD signal, +4.0 mdeg, for L-CCB and a negative one, −4.1 mdeg, for D-CCB. Other CD-active transitions are observed at shorter wavelengths: CD values of −2.9 mdeg at 280 nm and +2.9 mdeg at 250 nm for L-CCD and +3.6 mdeg at 280 nm and −3.0 mdeg at 250 nm for D-CCB. In contrast, The L-Arg ligand CD spectrum is characterised by a single positive band at 210–212 nm.[39] The anisotropic *g*-factors are used to evaluate the intrinsic chirality of the structures (Fig. S7, ESI†). The maximum values of the *g*-factor equal to $+1.60 \times 10^{-4}$ and -1.42×10^{-4} are determined from the peak in the band edge region (310 nm) for L and D-CCB. The unstructured signal observed at longer wavelength is likely related to a significant scattering contribution due to the micrometrical size of the crystals.

According to the SEM and TEM analyses, a morphological origin of the particle chirality can be excluded. Moreover, the XRD analysis confirms the orthorhombic centrosymmetric structure. Consequently, the origin of the particle chirality

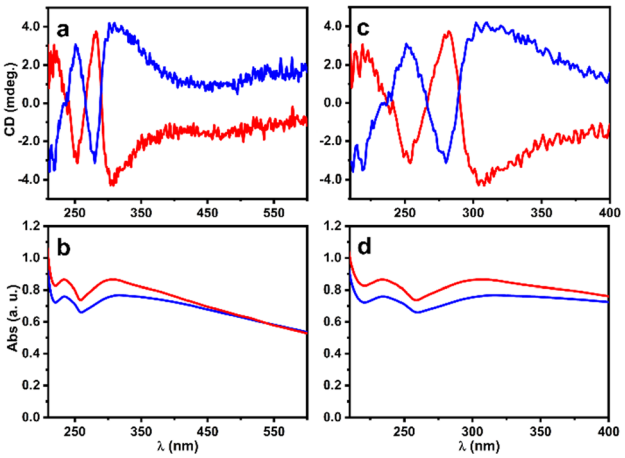

Fig. 5 Chiroptical characterisation of L-(blue) and D-(red) CCB colloidal dispersions. (a and b) CD (top) and UV/Vis spectra (bottom) in the 210 to 700 nm region, and (c and d) detail of the 210 to 400 nm region.

can be related to the effect of the chiral ligand adsorbed on the particle's surface. As reported above, ligand-induced chirality has been already observed in some examples of all-inorganic lead metal halides.[5–7]

To further investigate the origin of the chirality, a sample of $Cs_3Cu_2Br_5$ using L- or D-lysine (Lys) instead of arginine as the chiral ligand has been prepared. The CD analysis of the particles, produced in the presence of L- or D-Lys, reveals the successful chiral transfer (Fig. S8, ESI†). The analysis of a colloidal solution in isopropanol shows a similar signal to that of the arginine-stabilized sample. A similar pattern of the electronic transitions centred at 310, 280 and 250 nm is observed. However, the intensities of the CD transitions of the samples prepared using Lys are about five times lower relative to those of the Arg-stabilized counterpart (the g-factors at 310 nm of the samples prepared in the presence of L-Lys and D-Lys are 1.6×10^{-4} and -1.4×10^{-4}, respectively). This effect can be appreciated in Fig. S8 (ESI†) comparing the CD spectra of the samples produced in the presence of arginine and lysine. For all the samples an absorbance of 0.8 at 310 nm is used. This behaviour could be related to the multiple potential interactions mediated by hydrogen bonds established between the guanidium cation present in the Arg lateral chain and the bromide-rich surface of $Cs_3Cu_2Br_5$ microneedles, which promote the transfer of chirality.

In conclusion, a novel LARP approach to produce chiral $Cs_3Cu_2Br_5$ stabilised by L/D-arginine has been developed. The method allows the synthesis of chiral metal-halide particles *via* a single-step coprecipitation method in the presence of the chiral ligand. As evidenced by XRD and TEM, $Cs_3Cu_2Br_5$ particles show high phase purity and crystallinity. The morphology of the particles is characterised by the presence of microwires with a length of 5 μm and a lateral size of 100 nm. Metal halide crystals with anisotropic morphology are of wide interest for their application in photonics.[40,41] The optical properties show an emission centered at around 460 nm with a PLQY of 12.5%. These values are in good agreement with the activity of $Cs_3Cu_2Br_5$ prepared by other synthetic methods.[32,34,35]

The chiroptical investigation evidences the successful transfer of chirality by the presence of CD-active bands in the region corresponding to the band gap transition, around 300 nm. Anisotropic *g*-factors of 1.60×10^{-4} and -1.42×10^{-4}, determined for the particle in colloidal dispersion, are in-line with the hypothesis of a ligand-induced chirality mechanism. The lower chiroptical activity of $Cs_3Cu_2Br_5$ produced using lysine indicates an interesting efficiency of arginine in the transfer of chirality. This behavior could be associated with the multiple interactions *via* hydrogen bonds that can be established by the guanidinium group in the arginine lateral chain. We believe that this research will open up new strategies for the synthesis of new chiral micro- and nanomaterials with a range of important applications.

The authors would like to thank Science Foundation Ireland (grant number 20/FFP-A/8904). University of Verona, Italy, is gratefully acknowledged for funding in the framework of Joint Research 2022. The authors also wish to thank the Advanced Microscopy Laboratory, Trinity College, Dublin.

Conflicts of interest

There are no conflicts to declare.

References

1 J. Liu, L. Yang, P. Qin, S. Zhang, K. K. L. Yung and Z. Huang, *Adv. Mater.*, 2021, **33**, 2005506.
2 S. Jiang and N. A. Kotov, *Adv. Mater.*, 2022, 2108431.
3 X. Zhao, S. Q. Zang and X. Chen, *Chem. Soc. Rev.*, 2020, **49**, 2481–2503.
4 U. Hananel, A. Ben-Moshe, H. Diamant and G. Markovich, *Proc. Natl. Acc. Sci. U. S. A.*, 2019, **166**, 11159–11164.
5 T. He, J. Li, X. Li, C. Ren, Y. Luo, F. Zhao, R. Chen, X. Lin and J. Zhang, *Appl. Phys. Lett.*, 2017, **111**, 151102.
6 G. H. Debnath, Z. N. Georgieva, B. P. Bloom, S. Tan and D. H. Waldeck, *Nanoscale*, 2021, **13**, 15248–15256.
7 W. Chen, S. Zhang, M. Zhou, T. Zhao, X. Qin, X. Liu, M. Liu and P. Duan, *J. Phys. Chem. Lett.*, 2019, **10**, 3290–3295.
8 J. Ahn, E. Lee, J. Tan, W. Yang, B. Kim and J. Moon, *Mater. Horiz.*, 2017, **4**, 851–856.
9 J. Ahn, S. Ma, J. Y. Kim, J. Kyhm, W. Yang, J. A. Lim, N. A. Kotov and J. Moon, *J. Am. Chem. Soc.*, 2020, **142**, 4206–4212.
10 S. Ma, J. Ahn and J. Moon, *Adv. Mater.*, 2021, **33**, 2005760.
11 X. Li, X. Gao, X. Zhang, X. Shen, M. Lu, J. Wu, Z. Shi, V. L. Colvin, J. Hu, X. Bai, W. W. Yu and Y. Zhang, *Adv. Sci.*, 2021, **8**, 2003334.
12 F. Igbari, Z. K. Wang and L. S. Liao, *Adv. Energy Mater.*, 2019, **9**, 1803150.
13 Y. Li, Z. Zhou, N. Tewari, M. Ng, P. Geng, D. Chen, P. K. Ko, M. Qammar, L. Guo and J. E. Halpert, *Mat. Chem. Front.*, 2021, **5**, 4796–4820.
14 X. Zheng, J. Huang, Y. Liu, T. Wang, S. Han, Z. Wang, B. Teng and S. Ji, *Adv. Photonics Res.*, 2022, **3**, 2100289.
15 Z. Zhou, Y. Li, Z. Xing, H. H. Y. Sung, I. D. Williams, Z. Li, K. S. Wong and J. E. Halpert, *Adv. Mater. Interfaces*, 2021, **8**, 1–12.
16 T. Jun, K. Sim, S. Iimura, M. Sasase, H. Kamioka, J. Kim and H. Hosono, *Adv. Mater.*, 2018, **30**, 1804547.
17 Z. Ma, Z. Shi, C. C. Qin, M. Cui, D. Yang, X. Wang, L. Wang, X. Ji, X. Chen, J. Sun, D. Wu, Y. Zhang, X. J. Li, L. Zhang and C. Shan, *ACS Nano*, 2020, **14**, 4475–4486.
18 H. Chen, L. Zhu, C. Xue, P. Liu, X. Du, K. Wen, H. Zhang, L. Xu, C. Xiang, C. Lin, M. Qin, J. Zhang, T. Jiang, C. Yi, L. Cheng, C. Zhang, P. Yang, M. Niu, W. Xu, J. Lai, Y. Cao, J. Chang, H. Tian, Y. Jin, X. Lu, L. Jiang, N. Wang, W. Huang and J. Wang, *Nat. Commun.*, 2021, **12**, 1421.
19 X. Xu, S. Jiang, C. Fan, Q. Deng, L. Shen and Q. Zhang, *Adv. Opt. Mater.*, 2022, **10**, 2201107.
20 W. Q. Liang, Y. Li, J. L. Ma, Y. Wang, J. J. Yan, X. Chen, D. Wu, Y. T. Tian, X. J. Li and Z. F. Shi, *Nanoscale*, 2020, **12**, 17213–17221.
21 Z. X. Zhang, C. Li, Y. Lu, X. W. Tong, F. X. Liang, X. Y. Zhao, D. Wu, C. Xie and L. B. Luo, *J. Phys. Chem. Lett.*, 2019, **10**, 5343–5350.
22 J. Hui, P. Ran, Y. Su, L. Yang, X. Xu, T. Liu and Y. M. Yang, *J. Phys. Chem. C*, 2022, **126**, 12882–12888.
23 B. Wang, Z. Jia, X. Yang, S. Lu, J. Zhao, Z. Sun, Q. Qian, Q. Lin and Z. Zang, *Chem. Commun.*, 2022, **58**, 13206–13209.
24 M. Hunyadi, G. F. Samu, L. Csige, A. Csík, C. Buga and C. Janáky, *Adv. Funct. Mater.*, 2022, **32**, 2206645.
25 R. Duan, Z. Chen, D. Xiang, J. Si and X. Liu, *J. Lumin.*, 2023, **253**, 119482.
26 X. Zhao, A. Luo, Z. Lin, X. Zhong, Z. Zhu, Q. Lin and H. Su, *J. Lumin.*, 2023, **253**, 119434.
27 Z. Guo, J. Li, C. Wang, R. Liu, J. Liang, Y. Gao, J. Cheng, W. Zhang, X. Zhu, R. Pan and T. He, *Angew. Chem., Int. Ed.*, 2021, **60**, 8441–8445.
28 Y. Lu, Q. Wang, R. He, F. Zhou, X. Yang, D. Wang, H. Cao, W. He, F. Pan, Z. Yang and C. Song, *Angew. Chem., Int. Ed.*, 2021, **60**, 23578–23583.
29 F. Ge, B. H. Li, P. Cheng, G. Li, Z. Ren, J. Xu and X. H. Bu, *Angew. Chem., Int. Ed.*, 2022, **61**, e202115024.
30 T. Li, X. Mo, C. Peng, Q. Lu, C. Qi, X. Tao, Y. Ouyang and Y. Zhou, *Chem. Commun.*, 2019, **55**, 4554–4557.
31 Z. Dang, J. Shamsi, F. Palazon, M. Imran, Q. A. Akkerman, S. Park, G. Bertoni, M. Prato, R. Brescia and L. Manna, *ACS Nano*, 2017, **11**, 2124–2132.
32 Z. Luo, Q. Li, L. Zhang, X. Wu, L. Tan, C. Zou, Y. Liu and Z. Quan, *Small*, 2020, **16**, 1905226.
33 P. Sebastia-Luna, J. Navarro-Alapont, M. Sessolo, F. Palazon and H. J. Bolink, *Chem. Mater.*, 2019, **31**, 10205–10210.
34 G. K. Grandhi, N. S. M. Viswanath, H. Bin Cho, J. H. Han, S. M. Kim, S. Choi and W. Bin Im, *J. Phys. Chem. Lett.*, 2020, **11**, 7723–7729.
35 S. Fang, Y. Wang, H. Li, F. Fang, K. Jiang, Z. Liu, H. Li and Y. Shi, *J. Mater. Chem. C*, 2020, **8**, 4895–4901.
36 S. Li, J. Luo, J. Liu and J. Tang, *J. Phys. Chem. Lett.*, 2019, **10**, 1999–2007.
37 R. M. Webster, F. X. Kiemle, D. J. Bryce and J. Wiley, *Spettrometric Identification of Organic Compounds*, John Wiley & Sons, Chichester, 8th edn, 2005.
38 G. Socrates, *Infrared and Raman Characteristic Group Frequencies*, John Wiley & Sons, Chichester, 3rd edn, 2001.
39 N. Amdursky and M. M. Stevens, *Chem. Phys. Chem.*, 2015, **16**, 2768–2774.
40 S. Han, J. Quan, D. Wang, H. Li, X. Liu, J. Xu, Y. Zhang, Z. Li, L. Wu and X. Fang, *Adv. Sci.*, 2023, **10**, 1–9.
41 M. Ng, P. Geng, S. B. Shivarudraiah, L. Guo and J. E. Halpert, *Adv. Opt. Mater.*, 2022, **10**, 2201031.